Enhancement of Oxygen Mass Transfer Using Functionalized Magnetic Nanoparticles

Bernat Olle,* Seyda Bucak, Tracy C. Holmes, Lev Bromberg, T. Alan Hatton, and Daniel I. C. Wang

Department of Chemical Engineering, Massachusetts Institute of Technology, 77 Massachusetts Avenue, Cambridge, Massachusetts 02139

Oxygen-transfer enhancement has been observed in the presence of colloidal dispersions of magnetite (Fe_3O_4) nanoparticles coated with oleic acid and a polymerizable surfactant. These fluids improve gas–liquid oxygen mass transfer up to 6-fold (600%) at nanoparticle volume fractions below 1% in an agitated, sparged reactor and show remarkable stability in high-ionic strength media over a wide pH range. Through a combination of experiments using physical and chemical methods to characterize mass transfer, it is shown that (i) both the mass transfer coefficient (k_L) and the gas–liquid interfacial area (a) are enhanced in the presence of nanoparticles, the latter accounting for a large fraction of the total enhancement (80% or more), (ii) the enhancement in k_L measured by physical and chemical methods is similar and ranges from 20 to 60% approximately, (iii) the enhancement in k_L levels off at a nanoparticle volume fraction of approximately 1% v/v, and (iv) the enhancement in k_La shows a strong temperature dependence. These results are relevant to a wide range of processes limited by the mass transfer of a solute between a gas phase and a liquid phase, such as fermentation, waste treatment, and hydrogenation reactions.

Introduction

Absorption of gases into a liquid is of crucial importance to multiphase reactions because diffusion of a sparingly soluble gas species across a gas–liquid interface generally limits the reaction rates. Many examples of multiphase reactions have found application in the chemical and biochemical industries.[1] Typical applications include fermentation, water treatment, hydrogenation reactions, and the Fischer–Tropsch process.

The presence of particles or droplet emulsions in the liquid phase can enhance the rate of gas–liquid mass transfer when the solubility of the gas solute in the dispersed phase is higher than in the continuous liquid phase.[2–13] Several reviews have summarized the investigations undertaken in this area over the past 35 years.[1,14–16] In general, these investigations have only examined the effect on mass transfer of dispersed phases with particle or droplet size on the order of a few micrometers (μm) to several hundred μm.

This article considers the application of colloidal dispersions of magnetic nanoparticles to mass transfer enhancement in a gas–liquid system. The particle size studied is 3 orders of magnitude smaller than the typical size covered in the previous literature. The dispersions consisted of colloidal aqueous solutions of nanoparticles formed by a core of magnetite (Fe_3O_4) to which a first layer of oleic acid was grafted by chelating bonds to confer high oxygen storage capacity and a second layer of surfactant (Hitenol-BC) was covalently grafted to the first layer to prevent unbounded aggregation.

This technology shows potential for significant mass transfer enhancement in gas–liquid systems while addressing the limitations of former approaches based on the addition of an organic phase to aqueous media. In particular, it allows for the recovery of the dispersed phase after use through high-gradient magnetic separation (HGMS).[17,18] In addition, the nanoparticles are nonvolatile and are synthesized with benign, low-cost

chemicals, which makes their application attractive from environmental and economic standpoints.[19]

Colloidal dispersions of magnetic nanoparticles coated with different polymers have been used for separation of organic contaminants from water[20] and ion-exchange purification of proteins.[21] The common aspect in the applications listed is the exploitation of the large surface area per unit volume of the nanoparticle dispersions to accelerate the mass-transfer process.

Nanoparticles have been used for over a decade to increase the heat transfer properties of solutions in a wide range of heat transfer applications; the term *nanofluid*[22] has been coined to describe these dispersions. Research has shown that nanoparticles made of metals,[23–26] metal oxides,[27–29] and multiwalled carbon nanotubes[25,26] greatly enhance heat transfer in liquids. It is expected that these findings will have important repercussions in the microelectronics and transportation industry.[30] Nanoparticles of conducting materials have been found to enhance the thermal conductivity of base fluids to values well above the predictions of the theoretical effective property models,[31] which take into account the volume fraction of the particles but not their size. Determining the transport mechanisms involved in the anomalously enhanced heat transfer by nanoparticles has been the focus of many studies,[30,32–48] but to date, it remains a fundamental challenge.

Despite the research conducted on nanofluids for heat transfer, the potential application of nanofluids to mass-transfer enhancement has thus far been overlooked. Only one experimental study has been published,[49] where it was reported that nanometer-sized TiO_2 particles reduced the volumetric mass-transfer coefficient in a three-phase airlift reactor. Two theoretical studies[50,51] predicted that the presence of nanoparticles in a falling film exposed to air would enhance mass transfer but the improvements would not be significant. In contrast, the present work shows that aqueous solutions of nanoparticles can be used to increase oxygen mass transfer into water severalfold.

* To whom correspondence should be addressed. E-mail: bernat@mit.edu. Phone: 617 230 0734. Fax: 617 253 2400.

Experimental Methods

Nanoparticle Synthesis and Purification. A solution of 94 g of ferric chloride hexahydrate (97% FeCl$_3$·6H$_2$O, Sigma-Aldrich) and 34.4 g ferrous chloride tetrahydrate (99% FeCl$_2$·4H$_2$O, Sigma-Aldrich) in 100 g of water was stirred at 80 °C under nitrogen sparging for 30 min in a round-bottom flask. Next, 100 g of potassium oleate (40 wt % paste in water, CH$_3$(CH$_2$)$_7$CH=CH(CH$_2$)$_7$COOK, Sigma-Aldrich) was added, and the mixture was stirred for an additional 30 min. One hundred milliliters of an aqueous solution containing 28% ammonium hydroxide (NH$_4$OH, Mallinckrodt) was added to the mixture, after which the solution immediately turned black because of the formation of magnetite. The reaction continued at 80 °C under stirring and nitrogen sparging for 30 min, after which it was assumed that oleic acid had completely coated the magnetite aggregates. Following the coating of the magnetite aggregates, 100 g of Hitenol-BC (Daiichi Kogyo Seiyaki) and 5 g of ammonium persulfate (>98% (NH$_4$)$_2$S$_2$O$_8$, Sigma-Aldrich) were added to the reaction mixture. The reaction continued at 80 °C for 30 min, under nitrogen sparging and vigorous stirring, to allow for the formation of covalent bonds between the propenyl group of Hitenol-BC and the double bond in the alkyl chain of the oleic acid. Hitenol-BC is a polyoxyethylene alkylphenyl ether ammonium sulfate that contains a reactive propenyl group; the long PEO chains and the sulfate group confer stability in water when attached to the surface of oleic acid-coated magnetite particles. The solution was cooled to room temperature and was left in the oven at 80 °C overnight, after which most of the residual ammonium hydroxide evaporated. The dispersion was dialyzed against distilled water (14 000 kDa MWCO dialysis membrane, Pals) in a 20 L container under mild stirring for 2 days to remove unreacted potassium oleate, Hitenol-BC, ammonium persulfate, and other salts and metal ions. Finally, the dialyzed solution was kept in the oven overnight at 80 °C, after which its solid contents were measured. The final solid contents were typically between 15 and 25% in weight. This synthetic procedure yielded magnetic nanoparticles with an average number diameter between 20 and 25 nm.

Nanoparticle Characterization. The size of the magnetic nanoparticles was characterized by Dynamic Light Scattering (DLS) using a Brookhaven BI-200SM instrument at a measurement angle of 90°. Samples were first passed through a 0.45 μm filter to remove dust particles before the measurements were taken. A value of the diffusion coefficient is extracted from the autocorrelation function measured by DLS, and a hydrodynamic diameter is calculated using the Stokes–Einstein equation. Number-averaged and volume-averaged size distributions are recorded. The particle sizes cited in this work correspond to number averages. All measurements were recorded in quadruplicate and reported as average values.

ζ-potential measurements were recorded using a Brookhaven ZetaPals zeta potential analyzer. The built-in software uses the Smoluchowski potential model to convert electrophoretic mobility to ζ-potential. Measurements were recorded in quadruplicate and reported as average values. Measurements for both DLS and ζ-potential were conducted in 1000 ppm nanoparticle suspensions in fermentation media, the composition of which is described elsewhere,[19] with an ionic strength of approximately 1 M. The pH was adjusted with acetic acid or NaOH.

Experimental Determination of the Volumetric Mass-Transfer Coefficient ($k_L a$). Physical Method: Stirred Beaker as Experimental System to Determine k_L. Dynamic measurements of dissolved oxygen via surface aeration were used to determine k_L. Experiments were conducted in a cylindrical, 10.3

cm diameter beaker, without baffles, filled with 500 mL of liquid, to a liquid height of approximately 6 cm. The liquid was circulated slowly by a 4.5 cm diameter, 4-bladed, axial-flow impeller (pitched-blade with each blade measuring 3 cm wide and 1.5 cm long), placed centrally in the beaker. The free surface of the liquid remained flat (i.e., it did not exhibit a vortex or appear broken at the agitation speeds studied, 300 and 500 rpm). Dissolved oxygen was measured using a dissolved oxygen polarographic sensor (YSI 5010) connected to a data acquisition meter (YSI 5100). A built-in barometer compensated for slight atmospheric pressure variations between runs. The temperature was regulated at 37 ± 0.5 °C with a water bath, and the pH of the solution was adjusted to 7.0 before the start of the experiment. Oxygen response curves were obtained by first sparging nitrogen until the dissolved oxygen concentration fell to zero and then monitoring the increase in dissolved oxygen concentration resulting from the exposure of the liquid free surface to the room air. To ensure a constant gas–liquid interfacial area (83.3 cm^2), no air sparging was used during the second step. The relatively long duration of the experiments (~1 h) guaranteed that the time constant of the probe did not affect the response curves. The dissolved oxygen data can be analyzed by constructing a mass balance of oxygen in the liquid phase as follows
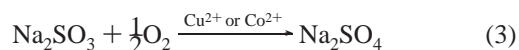
$$\frac{dC_{O_2,bulk}}{dt} = k_L a(C_{O_2}^* - C_{O_2,bulk}) = k_L a H(P_{O_2}^* - P_{O_2,bulk}) \quad (1)$$

where k_L is the liquid-side mass-transfer coefficient, a is the specific interfacial area, $P_{O_2,bulk}$ and $P_{O_2}^*$ are the partial pressures of oxygen in the well-mixed bulk and at saturation, respectively, $C_{O_2,bulk}$ and $C_{O_2}^*$ are the equivalent liquid-phase partial pressures, H is the Henry's law constant, and t is the elapsed time. Furthermore, it is assumed that the gas-side resistance to mass transfer is much lower than the liquid-side resistance. With $C_{O_2,bulk} = 0$ at $t = 0$, the integrated form of this expression is

$$\ln\left(1 - \frac{C_{O_2,bulk}}{C_{O_2}^*}\right) = -k_L a t \quad (2)$$

The rationale for characterizing mass transfer by a physical method in an agitated beaker is to avoid problems associated with interfacial area and gas holdup. By conducting experiments in a system that has a fixed and known gas–liquid contact area, we obtained information on the value of the mass-transfer coefficient, k_L.

Chemical Method: Sodium Sulfite Oxidation. Oxygen mass transfer was characterized in a laboratory-scale aerated and agitated fermentor using the sodium sulfite oxidation method,[52] which yields a steady state determination of the mass transfer rate. In the presence of a Cu^{2+} or Co^{2+} catalyst, sodium sulfite is oxidized according to the following reaction

$$Na_2SO_3 + \frac{1}{2}O_2 \xrightarrow{Cu^{2+} \text{ or } Co^{2+}} Na_2SO_4 \quad (3)$$

The reaction rate can be adjusted with temperature or by changing the catalyst concentration so that oxygen transport from the gas to the liquid, rather than the chemical reaction, is the limiting step. The oxygen uptake rate (OUR) is calculated by measuring the effluent-gas composition with a mass spectrometer (Perkin-Elmer MGA 1600) and performing a mass

balance on oxygen of the gas phase through the reactor as follows

$$OUR = \frac{F_{N_2,in}\left[\left(\dfrac{C_{O_2}}{C_{N_2}}\right)_{in} - \left(\dfrac{C_{O_2}}{C_{N_2}}\right)_{out}\right]}{V} \quad (4)$$

where OUR is the oxygen uptake rate, $F_{N_2,in}$ is the flowrate of nitrogen entering the reactor, C_{O_2} and C_{N_2} are the concentrations of oxygen and nitrogen, respectively, entering or exiting the reactor, and V is the working volume. The volumetric mass transfer coefficient can then be determined as

$$k_L a = \frac{OUR}{C_{O_2}^* - C_{O_2,bulk}} \quad (5)$$

where $C_{O_2}^*$ is the average liquid-phase saturation concentration in equilibrium with the inlet and outlet gas.

A convenient feature of this method is that separate determinations of the volumetric mass transfer coefficient $k_L a$ and the gas−liquid interfacial area a can be made by manipulating the relative magnitudes of the rate of chemical reaction and the rate of mass transfer.

The absorption flux of oxygen undergoing a pseudo-nth-order reaction with sulfite ions in an aqueous phase can be expressed as [53]

$$Na = a(C_{O_2}^* - C_{O_2,bulk})\sqrt{\frac{2}{n+1}k_n C_{O_2}^{*\,n-1}D_{O_2,L} + k_L^2} \quad (6)$$

where N is the absorption rate, a is the interfacial area, $D_{O_2,L}$ is the diffusion coefficient of oxygen in the liquid phase, k_n is the rate constant of the nth-order reaction, and n is the reaction order. The relative magnitudes of the rate of oxygen consumption by reaction and the rate of mass transfer can be compared through the Hatta number

$$Ha = \frac{\sqrt{\dfrac{2}{n+1}k_n C_{O_2}^{*\,n-1}D_{O_2,L}}}{k_L} \quad (7)$$

If the following conditions are met

$$C_{O_2,bulk} = 0 \quad (8a)$$

$$Ha < 0.3 \quad (8b)$$

$$Ha \ll C_{SO_3^{2-}}/(z C_{O_2}^*) \quad (8c)$$

where z is a stoichiometric coefficient (moles of sulfite reacted per mole of oxygen), then the reaction is limited by mass transfer and $k_L a$ can be obtained from oxygen absorption rates according to

$$Na = C_{O_2}^* k_L a \quad (9)$$

Experiments were performed in a 20 L (5.5 L working volume) stirred tank reactor (*Biolafitte* fermentor system, model BL 20.2). Only 5.5 L of working volume were used to reduce the amount of magnetic nanoparticles used at a given volume fraction. The fermentor was equipped with an Ingold-type pH electrode, a *Biolafitte* dissolved oxygen electrode, a temperature probe, a bottom aeration system consisting of a 4-branded rotating sparger, and an agitator with 3 Rushton 4-bladed turbine impellers (2 of the 3 impellers were covered by the liquid and

the third remained in the gas phase). A 0.67 M sodium sulfite solution was loaded into the reactor, and then a 1×10^{-3}M solution of copper sulfate catalyst was added. At this catalyst concentration, the mass transfer is not chemically enhanced.[54] The pH was initially adjusted to 8.0 with sulfuric acid to avoid the accelerated reaction regime typical of sodium sulfite solutions at higher pH. The temperature for the experimental runs was maintained at 37 ± 0.5 °C, except when specified otherwise.

Interfacial Area Determination. Experiments to determine the gas−liquid interfacial area were conducted with the experimental system previously described. The catalyst used was Co^{2+} instead of Cu^{2+} because it is not possible to attain an enhanced absorption regime with Cu^{2+};[52] instead, low Co^{2+} concentrations generally suffice. Interfacial areas can then be calculated from experimental measures of absorption rates.

The reaction rate of the oxidation of sodium sulfite can be manipulated through the catalyst concentration so that it becomes several times greater than the mass-transfer rate. The absorption rate is then greatly enhanced by the reaction, and the effect of the hydrodynamic conditions can be ignored. Under these conditions, the absorption rate depends only on the interfacial area and reaction kinetics, and thus eq 6 reduces to

$$Na = a C_{O_2}^*\sqrt{\frac{2}{n+1}k_n C_{O_2}^{*\,n-1}D_{O_2,L}} \quad (10)$$

The appropriate experimental conditions for determination of the interfacial area can be predicted if information on the kinetic constant of the reaction is available. However, adoption of literature data on kinetic constants for the sulfite oxidation is discouraged[52] because significant differences exist between measurements made at equivalent conditions by different authors. Alternatively, an appropriate range of catalyst concentrations that permit operation in a regime where absorption is kinetically enhanced can be selected. The interfacial area enhancement can then be quantified using eq 10, even if an accurate measure of the kinetic constant is not available. Rearranging eq 10 and taking a ratio in the presence and absence of particles, we obtained the following expression for the area enhancement

$$E_{area} = \frac{a_{nanoparticles}}{a_{control}} = \frac{(Na)_{nanoparticles}}{(Na)_{control}}\frac{(C_{O_2}^*\sqrt{C_{O_2}^{*\,n-1}})_{control}}{(C_{O_2}^*\sqrt{C_{O_2}^{*\,n-1}})_{nanoparticles}} \quad (11)$$

where the values of the kinetic constants and the diffusion coefficient initially present in eq 10 cancel. The $C_{O_2}^*$ terms do not cancel because the average value of the oxygen solubility depends on the oxygen partial pressure in the gas phase, which is not constant during the bubble residence time in the absorption equipment; instead, it decreases as the oxygen in the bubble is depleted.

Results

Characterization of Magnetic Nanoparticles. Stability in high-ionic strength media is a crucial requirement for magnetic nanoparticles to have practical applications in bioprocesses. The ζ-potential, which gives a measure of the surface charge of a particle, is a good indicator of the colloidal stability of a solution of particles. The nanoparticles synthesized in this study acquire stability in aqueous media by both electrostatic and steric interactions. Their exterior coating of Hitenol-BC contains a sulfonate group that confers a negative charge to the particle
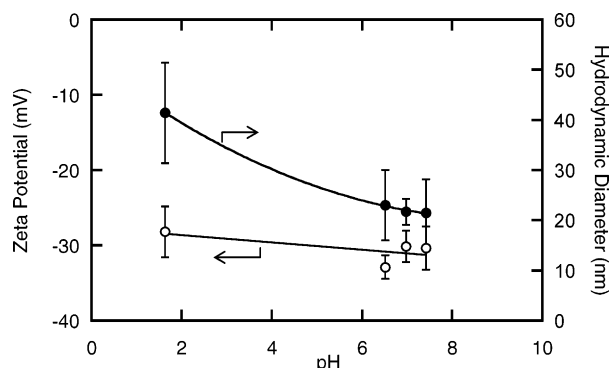
Figure 1. ζ-Potential and hydrodynamic diameter of particles as a function of pH.
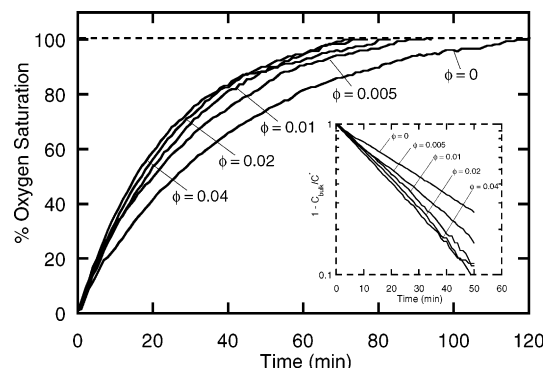

Figure 2. Response curves of dissolved oxygen in a stirred beaker at 300 rpm and at increasing nanoparticle holdup. Curves have been adjusted to a saturation value of 100%. The inset shows response curves on a semilogarithmic plot of dissolved oxygen at increasing nanoparticle holdup. The absolute value of the slope corresponds to the value of k_La.

surface. As shown in Figure 1, particles in fermentation media that has an ionic strength of approximately 1 M have a strongly negative ζ-potential of -30 mV in a pH range of 1.6$-$7.5; this indicates that the sulfonate groups on the surface remain deprotonated. In addition, the Hitenol-BC molecule contains an 8-unit PEO chain that is solvated by water molecules and confers steric stabilization. DLS measurements of the hydrodynamic diameter of the particles, which has a number average value of 20 nm over the range of pH relevant to fermentation (around 7), are also shown in Figure 1. This suggests that the particles are individually dispersed coated magnetite cores rather than clusters. The stability of the particles is still remarkable at a pH of 1.6, at which the particles experience some minor aggregation to form clusters of approximately 40 nm in diameter.

Mass-Transfer Characterization. Physical Method: Mass Transfer in a Stirred Beaker System. Oxygen mass transfer into an aqueous liquid phase is enhanced in the presence of nanoparticles, as shown in Figure 2. The time required to reach saturation is reduced by approximately 25% in the presence of a nanoparticle mass fraction of $\phi = 0.005$ (0.5% w/w). Further reductions are attained at larger particle holdups, but the effect is less pronounced above $\phi = 0.01$ (this effect is shown more clearly in Figure 3). The slopes of the first order curves shown in the inset on the semilogarithmic plot in Figure 2 are directly proportional to k_La and illustrate the increase of k_L in the presence of nanoparticles.

The absolute enhancement in k_L, defined as

$$E = \frac{k_{L,\text{nanoparticles}}}{k_{L,\text{control}}} \tag{12}$$

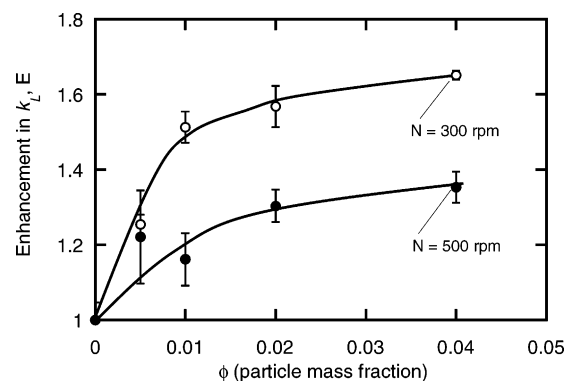is plotted in Figure 3 as a function of the nanoparticle holdup

Figure 3. Absolute enhancement in k_L as a function of nanoparticle holdup in a stirred beaker at different agitation rates.

Table 1. Physical Dimensions of the Reactor and Physical Properties of the System Used for the Determination of k_La by the Sodium Sulfite Method

tank diameter	21.7 cm
impeller diameter	9.8 cm
impeller type	2 Rushton turbines 4-bladed
liquid volume	5.5 L
liquid height	17 cm
oxygen diffusivity (37 °C)	3.22×10^{-9} m^2/s
oxygen solubility in 0.67 M SO$_3{}^{2-}$ (37 °C)^a	0.124 mol/m^3
viscosity (37 °C)^b	6.95×10^{-4} (Pa s)
surface tension (37 °C)^c	70 mN/m (40 mN/m with nanoparticles)

^{a} Estimated as $H = 5.909 \times 10^{-6} \exp((1602.1/T) - 0.9407C_{SO_3{}^{2-}}/(1 + 0.1933C_{SO_3{}^{2-}}))$.[52] ^{b} Measured using a U-tube Canon-Fenske. ^{c} Measured with a Kruss DSA10 instrument.

for different agitation rates. Data points are the average of 3 experiments. It can be observed that (i) enhancement increases rapidly at low particle holdups and slowly at larger holdups (above $\phi = 0.01$ approximately) and (ii) enhancement is greater at a lower agitation rate since the ratio of k_L values in the water control at the two agitation speeds studied, $k_{L,500\text{rpm}}/k_{L,300\text{rpm}}$, is larger than the equivalent ratio of k_L values in the presence of particles. The value of k_L in water increases by 67% upon changing the agitation speed (from 2.7×10^{-5} m/s at 300 rpm to 4.5×10^{-5} m/s at 500 rpm), whereas the value of k_L in the presence of particles increases by a smaller amount at any particle fraction (e.g., by 34% at $\phi = 0.01$).

Chemical Method: Sodium Sulfite Oxidation. This section presents measurements of mass-transfer enhancement over a range of values of power input, superficial velocity, and nanoparticle mass fraction obtained using the sodium sulfite method. A comprehensive review of the method has been presented elsewhere.[52]

Determination of the Volumetric Mass Transfer Coefficient (k_La). The physical dimensions of the absorption equipment and the fluid properties used for the determination of k_La are summarized in Table 1. In the presence of a 1×10^{-3} M concentration of Cu^{2+} catalyst, the rate of reaction is fast enough to maintain the dissolved oxygen levels in the bulk at zero, $C_{\text{O}_2,\text{bulk}} = 0$ (except for a brief induction time at the beginning of the experiments, during which the cuprous ions are being formed), as indicated by readings from a dissolved oxygen probe. Yet, the chemical enhancement of the absorption rate caused by the catalyst is not enough to obtain a fast-reaction regime[55] in which absorption rates would depend solely on reaction kinetics and not on mass transfer. Using a value for the kinetic constant, k_n, of 3.5 s^{-1},[56] the diffusion coefficient of oxygen listed in Table 1, a value of $n = 2$,[57,58] and typical
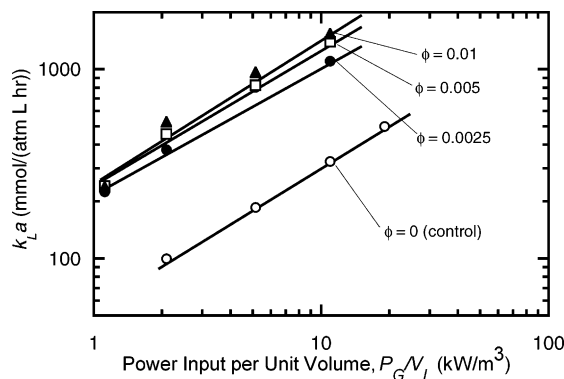
Figure 4. Volumetric mass-transfer coefficients measured by the sodium sulfite method as a function of power input per unit volume at several nanoparticle mass fractions. Operating conditions are $T = 37$ °C, pH = 8.0, $V_s = 14.5$ cm/min.
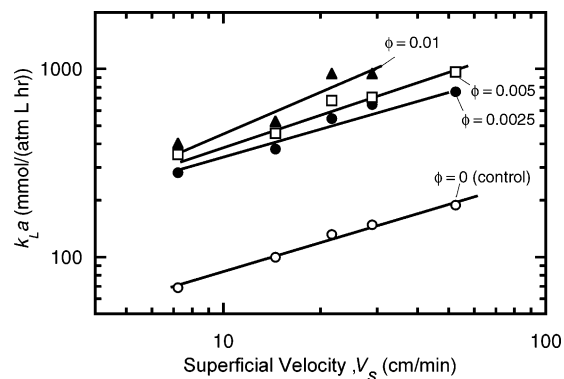

Figure 5. Volumetric mass-transfer coefficients measured by the sodium sulfite method as a function of superficial velocity at several nanoparticle mass fractions. Operating conditions are $T = 37$ °C, pH = 8.0, $P_G/V_L = 2.1$ kW/m^3.

Figure 6. Absolute enhancement in $k_L a$ measured by the sodium sulfite method as a function of power input per unit volume at several nanoparticle holdups. Operating conditions are $T = 37$ °C, pH = 8.0, $V_s = 14.5$ cm/min.

Figure 7. Absolute enhancement in $k_L a$ measured by the sodium sulfite method as a function of superficial velocity at several nanoparticle holdups. Operating conditions are $T = 37$ °C, pH = 8.0, $P_G/V_L = 2.1$ kW/m^3.

Figure 8. Comparison of calculated $k_L a$ values with experimental data.

values of k_L in the absorption equipment calculated from an eddy model by Lamont,[59] which range from 5×10^{-4} to 8.3×10^{-4} m/s for the experimental conditions of agitation studied, we found that the values of the Hatta number calculated from eq 7 range from 0.21 to 0.13. Additionally, the term $C_{SO_3^{2-}}/(zC_{O_2}^*)$ has a value of 2700 for a 0.67 M sodium sulfite solution. Therefore, the constraints imposed by eqs 8a, 8b, and 8c are satisfied.

The results presented in Figures 4 and 5 show that a 3- to 4-fold enhancement of $k_L a$ can be obtained at a particle mass fraction as low as $\phi = 0.0025$ (0.25% w/v). At higher particle concentrations, $k_L a$ can still be further enhanced, but diminishing returns are obtained as the particle fraction approaches $\phi = 0.01$. The results illustrate that a severalfold enhancement can be obtained over a broad range of operating conditions of power input per unit volume and superficial velocity. Figures 6 and 7 show the influence of power input per unit volume and superficial velocity on the absolute enhancement in $k_L a$ defined as

$$E' = \frac{(k_L a)_{\text{nanoparticles}}}{(k_L a)_{\text{control}}} \qquad (13)$$

It is apparent from Figure 6 that enhancement initially increases with power input, reaches a maximum, and subsequently decreases. As will be shown in the next section, this trend is caused by the change in interfacial area enhancement as a function of power input. As shown in Figure 7, superficial velocity does not have a noticeable effect on enhancement.
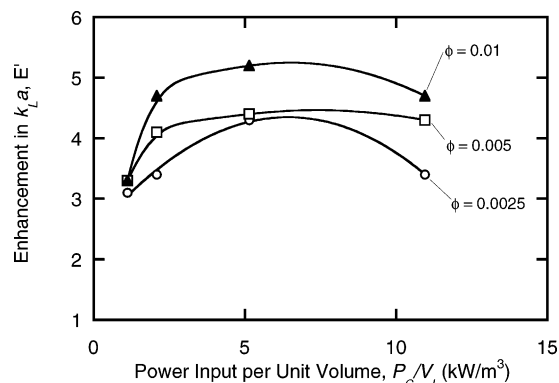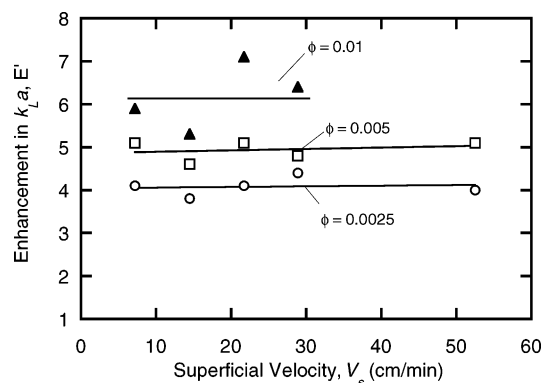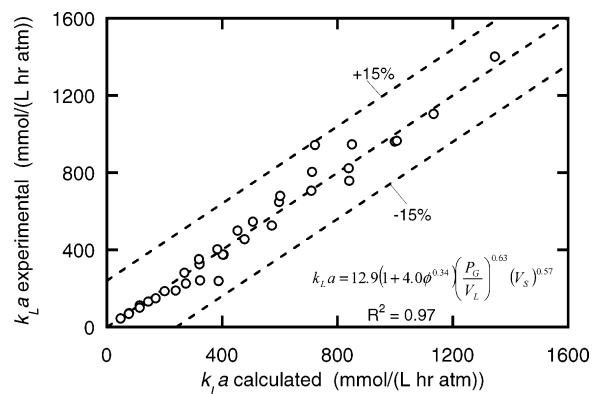
Through a nonlinear least-squares fit of all data presented in Figures 4 and 5, an empirical correlation for $k_L a$ as a function of particle mass fraction, power input per unit volume, and superficial velocity is obtained

$$k_L a = a(1 + b\phi^c)\left(\frac{P_G}{V_L}\right)^d (V_S)^e \qquad (14)$$

where the values of the estimated parameters are $a = 12.9 \pm 5.1$, $b = 4.0 \pm 1.0$, $c = 0.34 \pm 0.09$, $d = 0.63 \pm 0.05$, and $e = 0.57 \pm 0.09$ (95% confidence intervals), P_G/V_L is the gassed power per unit volume, and V_S is the superficial gas velocity. As shown in Figure 8, eq 14 gives a satisfactory correlation of all data. This correlation can be used for scale-up purposes but does not contain physical insight into the mechanism of mass transfer enhancement by nanoparticles.
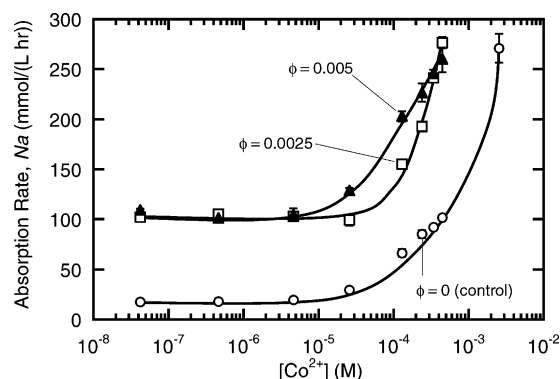
Figure 9. Absorption rate as a function of cobalt ion concentration at pH = 8.5, $T = 37$ °C, $P_G/V_L = 2.1$ kW/m^3, $V_s = 14.5$ cm/min, and $[SO_3^{2-}] = 0.67$ M. Above $[Co]^{2+} = 10^{-5}$ M, the absorption rate is enhanced by the chemical reaction.

Determination of the Interfacial Area (*a*). An appropriate range of catalyst concentrations that permit operation in a regime where absorption is kinetically enhanced was selected by performing absorption experiments at increasing catalyst concentration, as shown in Figure 9. It is found that above a concentration of Co^{2+} of 1×10^{-5} M, the absorption rate increases with catalyst concentration. This observation is equally valid in the presence of nanoparticles at mass fractions of $\phi = 0.0025$ and 0.005. Inspection of Figure 9 reveals that nanoparticles increase the gas−liquid interfacial area; it also reveals that doubling the nanoparticle mass fraction, from $\phi = 0.0025$ to 0.005, does not have a significant effect on the interfacial area. These considerations are made under the assumption that nanoparticles do not alter the kinetic reaction rate of the sodium sulfite oxidation.

Above a catalyst concentration of 10^{-4} M (Figure 9), where mass transfer is greatly enhanced by the chemical reaction, the average value of area enhancement is 3.1 ± 0.5 (as calculated from eq 11) in the presence of $\phi = 0.0025$ mass fraction of nanoparticles, at $P_G/V_L = 2.1$ kW/m^3, and $V_S = 14.5$ cm/min. For $\phi = 0.005$, this value is 3.4 ± 0.2. At equivalent conditions of power input and superficial velocity, the corresponding enhancement in $k_L a$ (Figure 6) is 3.4 for $\phi = 0.0025$ and 4.1 for $\phi = 0.005$. Therefore, for this particular experimental condition, most of the enhancement in $k_L a$ is caused by an increase in the interfacial area.

A quantitative analysis of the relative contribution of area effects to the total enhancement in $k_L a$ has been made by performing interfacial area measurements for the range of conditions presented in Figures 4 and 5. Estimations of area enhancement have been made as described previously for a nanoparticle mass fraction of $\phi = 0.0025$, and the results are summarized in Figures 10 and 11. The shapes of the interfacial area enhancement curve and the $k_L a$ enhancement curve as functions of power input for $\phi = 0.0025$ closely resemble each other; this indicates that the $k_L a$ enhancement trend, an initial increase at low power input followed by a decrease above approximately 6 kW/m^3, is caused primarily by a change in interfacial area rather than a change in k_L. Figure 10 further shows that (i) enhancement in k_L, given by the ratio of the $k_L a$ enhancement to the a enhancement, also contributes to total $k_L a$ enhancement and (ii) the fraction of the total $k_L a$ enhancement corresponding to changes in k_L decreases with power input; therefore, the higher the base mass-transfer coefficient, the lower the enhancement in k_L. Both these observations are consistent with the data obtained by a physical method in a stirred beaker presented in Figure 3. Enhancement data as a function of superficial velocity, shown in Figure 11, do not show as clear
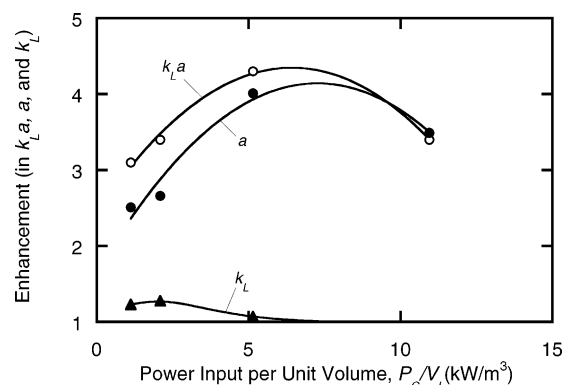

Figure 10. Enhancement in $k_L a$, a, and k_L as a function of power input per unit volume for $\phi = 0.0025$ at $V_s = 14.5$ cm/min, pH = 8.0, T = 37 °C. The enhancement in k_L is calculated as $E_{k_L} = E_{k_L a}/E_a$.
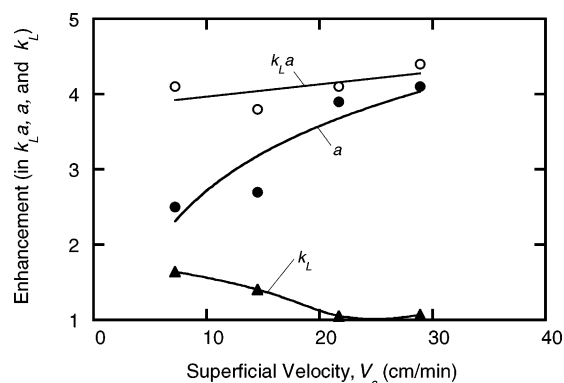

Figure 11. Enhancement in $k_L a$, a, and k_L as a function of superficial velocity for $\phi = 0.0025$ at $P_G/V_L = 2.1$ kW/m^3. The enhancement in k_L is calculated as $E_{k_L} = E_{k_L a}/E_a$.
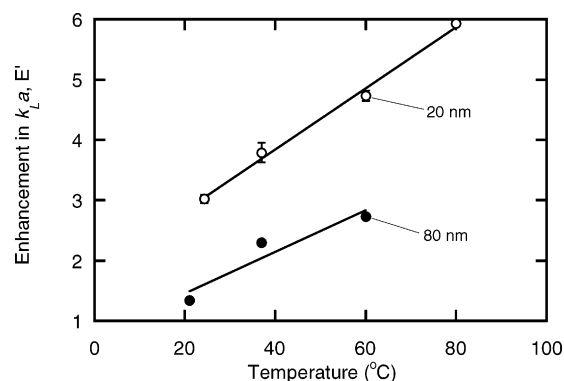

Figure 12. Enhancement in $k_L a$ as a function temperature for 80 nm, PPO−PEO-coated particles and 20 nm oleic acid-coated particles.

a pattern; while the $k_L a$ enhancement remains approximately constant as a function of superficial velocity, area enhancement increases with superficial velocity, probably as a result of higher holdup.

Effect of Temperature on Enhancement. The effect of temperature on the mass-transfer coefficient in aqueous solutions was investigated for two types of nanoparticles: (i) 20 nm particles synthesized as described in the Experimental Section and (ii) 80 nm clusters of magnetite cores coated with random copolymers of ethylene oxide (EO) and propylene oxide (PO) repeat units, the synthesis method of which has been described elsewhere.[60,61] A range of temperatures from 20 to 80 °C was explored at $P_G/V_L = 2.1$ kW/m^3, $V_S = 14.5$ cm/min, and $\phi = 0.0025$ for both types of particles. Figure 12 shows the experimental enhancement in $k_L a$ (eq 13) as a function of temperature. A strong temperature dependence is evident for

both types of particles: a 3- to 6-fold enhancement of k_La takes place from 25 to 80 °C in the presence of $\phi = 0.0025$ oleic acid-coated particles, whereas a 1.3- to 2.7-fold enhancement of k_La takes place from 20 to 60 °C in the presence of $\phi = 0.0025$ PPO−PEO-coated particles.

Discussion

Measurements obtained by the physical method (Figure 3) and the chemical method (Figure 10) show that the enhancement corresponding to k_L effects that can be obtained at a nanoparticle mass fraction below $\phi = 0.01$ is below 1-fold (approximately 25% for both the physical method experiments and chemical method experiments). It is also shown that k_L enhancement decreases with power input.

The effect of nanoparticles on interfacial area is clear at all concentrations considered, down to a nanoparticle mass fraction of $\phi = 0.0025$. Doubling this fraction, as shown in Figure 9, does not have a significant effect on the interfacial area enhancement. This is consistent with surface tension measurements conducted in a Kruss DSA10 instrument that have shown that nanoparticles at a mass fraction of $\phi = 0.001$ reduce the surface tension of an aqueous solution to approximately 40 mN/m (30 mN/m below the value for pure water at 37 °C). Increasing the particle fraction above $\phi = 0.001$ has a negligible effect on the surface tension reduction of a sample. While the trends are consistent, the values of area that can be predicted from correlations[62] (using these surface tension values in the presence of nanoparticles) largely underestimate the area measurements in this work.

The exponents d and e on the power input and superficial velocity for expressions of the form of eq 14 are typically 0.4 and 0.5 for water-coalescing systems and 0.7 and 0.2 for water-noncoalescing systems.[63] The value of $d = 0.63 \pm 0.05$ estimated in this work falls between the values of coalescing and noncoalescing systems and the value of $e = 0.57 \pm 0.09$ is similar to that of coalescing systems. It is likely that nanoparticles modify the coalescencing behavior of the medium, given the substantial effect that they have on interfacial area and surface tension.

The enhancement of k_La as a function of temperature shown in Figure 12 cannot be an effect of temperature on oxygen diffusivity or solubility. Although diffusivity of oxygen increases with temperature, its solubility in water decreases, and overall, oxygen uptake rates in water as a function of temperature vary only slightly. The enhancement trends as a function of temperature are not a product of the differential solubility (or temperature dependence of solubility) of oxygen in oleic acid and PPO−PEO copolymers, either. Although the solubility of oxygen in oleic acid is 4 times higher than in water, the dispersions used cannot solubilize significantly more oxygen than pure water: a solution with mass fraction $\phi = 0.0025$ of oleic acid-coated nanoparticles contains approximately a mass fraction of oleic acid, ϕ_{oleic}, of [$(0.2)(0.0025) = 5 \times 10^{-4}$], which can account for only [$(5 \times 10^{-4})4] = 0.002$ (0.2%) of the total amount of oxygen solubilized in the media. PPO−PEO copolymers are not reportedly known as oxygen carriers. The unambiguous temperature dependence of the enhancement suggests one of the following: (i) the enhancement in interfacial area caused by nanoparticles is greater at a higher temperature, (ii) the enhancement in k_L is greater at a higher temperature, or (iii) both. A possible mechanism at play could be enhancement in k_L caused by Brownian motion of the nanoparticles: diffusivity of a nanoparticle increases with temperature and decreases with particle size, in qualitative agreement with data in Figure

12. Further experiments using the physical and chemical methods to determine separately the impact of temperature on k_L and a could be used to clarify this point.

The temperature effect on mass-transfer enhancement presented in Figure 12 is qualitatively similar to a temperature effect on enhancement of heat transfer by nanofluids reported in the literature,[27] which also shows a linear dependence. However, it must be noted that (i) the absolute value of the mass transfer enhancement reported here is 1 order of magnitude greater than the heat transfer enhancement reported in the literature and (ii) the experimental equipment used is widely different. While the comparison is appealing, given the analogy between heat and mass transfer, further evidence would be necessary to conclude that the underlying mechanisms of enhanced transfer, which themselves are as yet unknown, are analogous.

The enhancement in k_L measured by both the physical and chemical methods cannot be predicted satisfactorily using mass-transfer models for dispersed phases available in the literature.[12] Such models predict a linear increase of the enhancement with the volume fraction of the dispersed phase, which, as shown in Figure 3, is not true for the nanoparticles studied in this work. These models also largely underestimate the enhancement resulting from the presence of dispersed nanoparticles. Similarly, research focusing on heat transfer[30] has indicated the failure of theoretical effective property models[31] to predict experimental data of enhanced heat transfer in nanofluids. The mechanism by which nanoparticles increase the interfacial area and the mass-transfer coefficient is still unclear and work is ongoing in an attempt to resolve this issue.

Conclusions

We have presented a new type of dispersion with remarkable stability in high-ionic strength solutions (1 M) and over a wide range of pH conditions that can be used to enhance gas−liquid oxygen mass transfer up to 6-fold. These findings have direct implications for the field of fermentation. We are currently using nanoparticle dispersions to enhance the oxygen-uptake rate and cell density in bacterial cultures.

Through a combination of experiments using a dynamic method (surface aeration) and a steady-state method (sodium sulfite oxidation), we have shown that both the mass-transfer coefficient and the interfacial area are enhanced in the presence of nanoparticles, and that the latter accounts for most of the total enhancement. Further, the enhancement in k_L increases rapidly at low nanoparticle holdups and slowly above $\phi = 0.01$ (approximately). Finally, it has been observed that the enhancement in k_La shows a strong temperature dependence. On the basis of these results, our future investigations will attempt to elucidate the mechanism by which nanoparticles increase the gas−liquid interfacial area and the mass transfer coefficient.

Acknowledgment

Nomenclature

a, b, c, d, e = parameters of eq 14

a = specific interfacial area, m^{-1}

$C_{O_2,bulk}$ = liquid-phase concentration of oxygen in the well-mixed bulk, mol m^{-3}

$C_{O_2}^*$ = liquid-phase concentration of oxygen at saturation (eq 1) or the average liquid-phase concentration of oxygen in equilibrium with the inlet and outlet gas (eq 5), mol m^{-3}

C_{O_2} = concentration of oxygen entering the reactor, mol m^{-3}

C_{N_2} = concentration of nitrogen entering or exiting the reactor, mol m^{-3}

$D_{O_2,L}$ = diffusion coefficient of oxygen in the liquid phase, m^2 s^{-1}

E = absolute enhancement in k_L

E' = absolute enhancement in $k_L a$

E_{area} = absolute enhancement in interfacial area

$F_{N_2,in}$ = flow rate of nitrogen entering the reactor, m^3 s^{-1}

H = Henry's law constant, mol m^{-3} Pa^{-1}

Ha = Hatta number

k_L = liquid-side mass-transfer coefficient, m s^{-1}

$k_L a$ = volumetric mass-transfer coefficient, s^{-1}

k_n = rate constant of nth-order reaction, m^3 mol^{-1} s^{-1} for n = 2

N = absorption rate, mol m^{-2} s^{-1}

n = reaction order

OUR = oxygen uptake rate, mol m^{-3} s^{-1}

$P_{O_2,bulk}$ = partial pressure of oxygen in the well-mixed bulk, Pa

$P_{O_2}^*$ = partial pressure of oxygen at saturation, Pa

P_G/V_L = gassed power input per unit volume, kW m^{-3}

t = time, s

V = volume, m^3

V_s = superficial gas velocity, m s^{-1} (shown in cm/min in figures to facilitate reading)

z = stoichiometric coefficient (moles of sulfite reacted per mole of oxygen)

Greek Symbols

ϕ = volume fraction of nanoparticles

Literature Cited

(1) Kim, S.; Kang, Y. Heat and mass transfer in three-phase fluidized-bed reactors—An overview. *Chem. Eng. Sci.* **1997**, *52* (21–22), 3639–3660.

(2) Alper, E.; Wichtendahl, B.; Deckwer, W. Gas-absorption mechanism in catalytic slurry reactors. *Chem. Eng. Sci.* **1980**, *35* (1–2), 217–222.

(3) Damiano, D.; Wang, S. S. Novel use of a perfluorocarbon for supplying oxygen to aerobic submerged cultures. *Biotechnol. Lett.* **1985**, *7* (2), 81–86.

(4) Junker, B.; Hatton, T.; Wang, D. Oxygen-transfer enhancement in aqueous perfluorocarbon fermentation systems. 1. Experimental-observations. *Biotechnol. Bioeng.* **1990**, *35* (6), 578–585.

(5) Kars, R.; Best, R.; Drinkenburg, A. Sorption of propane in slurries of active-carbon in water. *Chem. Eng. J. Biochem. Eng.* **1979**, *17* (3), 201–210.

(6) Linek, V.; Benes, P. Study of mechanism of gas absorption into oil–water emulsions. *Chem. Eng. Sci.* **1976**, *31* (11), 1037–1046.

(7) Mattiasson, B.; Adlercreutz, P. Perfluorochemicals in biotechnology. *Trends Biotechnol.* **1987**, *5* (9), 250–254.

(8) Mattiasson, B.; Adlercreutz, P. Use of perfluorochemicals for oxygen-supply to immobilized cells. *Ann. NY Acad. Sci.* **1983**, *413* (Dec), 545–547.

(9) McMillan, J. D.; Wang, D. I. C. Enhanced oxygen-transfer using oil-in-water dispersions. *Ann. NY Acad. Sci.* **1987**, *506*, 569–582.

(10) Mimura, A.; Kawano, T.; Kodaira, R. Biochemical engineering analysis of hydrocarbon fermentation. I. Oxygen transfer in the oil–water system. *J. Ferment. Technol.* **1969**, *47*, 229–236.

(11) Yoshida, F.; Yamane, T.; Miyamoto, Y. Oxygen absorption into oil-in-water emulsion: A study of hydrocarbon fermentors. *Ind. Eng. Chem. Process Des. Dev.* **1970**, *9* (4), 570–577.

(12) Mehra, A. Intensification of multiphase reactions through the use of a microphase. 1. Theoretical. *Chem. Eng. Sci.* **1988**, *43* (4), 899–912.

(13) Mehra, A.; Pandit, A.; Sharma, M. Intensification of multiphase reactions through the use of a microphase. 2. Experimental. *Chem. Eng. Sci.* **1988**, *43* (4), 913–927.

(14) Beenackers, A.; Vanswaaij, W. Mass-transfer in gas–liquid slurry reactors. *Chem. Eng. Sci.* **1993**, *48* (18), 3109–3139.

(15) Dumont, E.; Delmas, H. Mass transfer enhancement of gas absorption in oil-in-water systems: A review. *Chem. Eng. Process* **2003**, *42* (6), 419–438.

(16) Lowe, K.; Davey, M.; Power, J. Perfluorochemicals: Their applications and benefits to cell culture. *Trends Biotechnol.* **1998**, *16* (6), 272–277.

(17) Ditsch, A.; Lindenmann, S.; Laibins, P.; Wang, D.; Hatton, T. High-gradient magnetic separation of magnetic nanoclusters. *Ind. Eng. Chem. Res.* **2005**, ASAP Article.

(18) Moeser, G. D.; Roach, K. A.; Green, W. H.; Hatton, T. A.; Laibinis, P. E. High-gradient magnetic separation of coated magnetic nanoparticles. *AIChE J.* **2004**, *50* (11), 2835–2848.

(19) Bromberg, L.; Yin, J.; Wang, D.; Hatton, T. A.; Olle, B. Bioprocesses enhanced by fluoropolymer-coated magnetic nanoparticles and methods related thereto. US patent application, 2004.

(20) Moeser, G.; Roach, K.; Green, W.; Laibinis, P.; Hatton, T. Water-based magnetic fluids as extractants for synthetic organic compounds. *Ind. Eng. Chem. Res.* **2002**, *41* (19), 4739–4749.

(21) Ditsch, A.; Wang, D. I. C.; Hatton, T. A. Magnetic fluids for ion-exchange purification of recombinant proteins. *Abstr. Pap. Am. Chem. Soc.* **2004**, *227*, U211–U211.

(22) Choi, S. Enhancing thermal conductivity of fluids with nanoparticles. In *Development and Applications of Non-Newtonian Flows*; American Society of Mechanical Engineers: Washington, DC, 1995; pp 99–105.

(23) Eastman, J.; Choi, S.; Li, S.; Yu, W.; Thompson, L. Anomalously increased effective thermal conductivities of ethylene glycol-based nanofluids containing copper nanoparticles. *Appl. Phys. Lett.* **2001**, *78* (6), 718–720.

(24) Patel, H.; Das, S.; Sundararajan, T.; Sreekumaran Nair, A.; George, B.; Pradeep, T. Thermal conductivities of naked and monolayer protected metal nanoparticle based nanofluids: Manifestation of anomalous enhancement and chemical effects. *Appl. Phys. Lett.* **2003**, *83* (14), 2931–2933.

(25) Choi, S.; Zhang, Z.; Yu, W.; Lockwood, F.; Grulke, E. Anomalous thermal conductivity enhancement in nanotube suspensions. *Appl. Phys. Lett.* **2001**, *79* (14), 2252–2254.

(26) Xie, H.; Lee, H.; Youn, W.; Choi, M. Nanofluids containing multiwalled carbon nanotubes and their enhanced thermal conductivities. *J. Appl. Phys.* **2003**, *94* (8), 4967–4971.

(27) Das, S.; Putra, N.; Thiesen, P.; Roetzel, W. Temperature dependence of thermal conductivity enhancement for nanofluids. *J. Heat Transfer* **2003**, *125* (4), 567–574.

(28) Lee, S.; Choi, S.; Li, S.; Eastman, J. Measuring thermal conductivity of fluids containing oxide nanoparticles. *J Heat Transfer* **1999**, *121* (2), 280–289.

(29) Masuda, H.; Ebata, A.; Teramae, K.; Hishinuma, N. Alteration of thermal conductivity and viscosity of liquid by dispersing ultra-fine particles. *Netsu Bussei (Japan)* **1993**, *4* (4), 227–233.

(30) Eastman, J.; Phillpot, S.; Choi, S.; Keblinski, P. Thermal transport in nanofluids. *Annu. Rev. Mater. Res.* **2004**, *34*, 219–246.

(31) Hamilton, R.; Crosser, O. Thermal conductivity of heterogeneous two-component systems. *Ind. Eng. Chem. Fundam.* **1962**, *1*, 187–191.

(32) Bhattacharya, P.; Saha, S.; Yadav, A.; Phelan, P.; Prasher, R. Brownian dynamics simulation to determine the effective thermal conductivity of nanofluids. *J. Appl. Phys.* **2004**, *95* (11), 6492–6494.

(33) Jang, S.; Choi, S. Role of brownian motion in the enhanced thermal conductivity of nanofluids. *Appl. Phys. Lett.* **2004**, *84* (21), 4316–4318.

(34) Keblinski, P.; Phillpot, S.; Choi, S.; Eastman, J. Mechanisms of heat flow in suspensions of nanosized particles (nanofluids). *Int. J. Heat Mass Transfer* **2002**, *45* (4), 855–863.

(35) Koo, J.; Kleinstreuer, C. A new thermal conductivity model for nanofluids. *J. Nanopart. Res.* **2004**, *6* (6), 577–588.

(36) Kumar, D.; Patel, H.; Kumar, V.; Sundararajan, T.; Pradeep, T.; Das, S. Model for heat conduction in nanofluids. *Phys. Rev. Lett.* **2004**, *93* (14), 144301.

(37) Prasher, R.; Bhattacharya, P.; Phelan, P. Thermal conductivity of nanoscale colloidal solutions (nanofluids). *Phys. Rev. Lett.* **2005**, *94* (2), 025901.

(38) Wang, B.; Zhou, L.; Peng, X. A fractal model for predicting the effective thermal conductivity of liquid with suspension of nanoparticles. *Int. J. Heat Mass Transfer* **2003**, *46* (14), 2665–2672.

(39) Wen, D.; Ding, Y. Effect on heat transfer of particle migration in suspensions of nanoparticles flowing through minichannels. Proceedings of the Second International Conference on Microchannels and Minichannels (ICMM2004), Rochester, NY, 2004.

(40) Xuan, Y.; Roetzel, W. Conceptions for heat transfer correlation of nanofluids. *Int. J. Heat Mass Transfer* **2000**, *43* (19), 3701–3707.

(41) Xuan, Y.; Yao, Z. Lattice boltzmann model for nanofluids. *Heat Mass Transfer* **2005**, *41* (3), 199–205.

(42) Xuan, Y.; Yu, K.; Li, Q. Investigation on flow and heat transfer of nanofluids by the thermal lattice Boltzmann model. *Prog. Comput. Fluid Dyn.* **2005**, *5* (1–2), 13–19.

(43) Xue, L.; Keblinski, P.; Phillpot, S.; Choi, S.; Eastman, J. Effect of liquid layering at the liquid−solid interface on thermal transport. *Int. J. Heat Mass Transfer* **2004**, *47* (19−20), 4277−4284.

(44) Xue, Q. Model for effective thermal conductivity of nanofluids. *Phys. Lett. A* **2003**, *307* (5−6), 313−317.

(45) Xue, Q.; Xu, W. A model of thermal conductivity of nanofluids with interfacial shells. *Mater. Chem. Phys.* **2005**, *90* (2−3), 298−301.

(46) Yu, W. Stable and highly conductive nanofluids−experimental and theoretical studies. Proceedings of the 6th ASME−JSME Thermal Engineering Joint Conference, 2003.

(47) Yu, W.; Choi, S. An effective thermal conductivity model of nanofluids with a cubical arrangement of spherical particles. *J. Nanosci. Nanotechnol.* **2005**, *5* (4), 580−586.

(48) Yu, W.; Choi, S. The role of interfacial layers in the enhanced thermal conductivity of nanofluids: A renovated Hamilton-crosser model. *J. Nanopart. Res.* **2004**, *6* (4), 355−361.

(49) Wen, J.; Jia, X.; Feng, W. Hydrodynamic and mass transfer of gas−liquid−solid three-phase internal loop airlift reactors with nanometer solid particles. *Chem. Eng. Technol.* **2005**, *28* (1), 53−60.

(50) Ali, A.; Vafai, K. An investigation of heat and mass transfer between air and desiccant film in an inclined parallel and counter flow channels. *Int. J. Heat Mass Transfer* **2004**, *47* (8−9), 1745−1760.

(51) Ali, A.; Vafai, K.; Khaled, A. Analysis of heat and mass transfer between air and falling film in a cross-flow configuration. *Int. J. Heat Mass Transfer* **2004**, *47* (4), 743−755.

(52) Linek, V.; Vacek, V. Chemical-engineering use of catalyzed sulfite oxidation-kinetics for the determination of mass-transfer characteristics of gas−liquid contactors. *Chem. Eng. Sci.* **1981**, *36* (11), 1747−1768.

(53) Danckwerts, P. *Gas−liquid reactions*; McGraw-Hill: New York, 1970.

(54) Linek, V. Bestimmung der Phasen-Grenzflache in einem mit mechanischem Ruhrwerk versehenen Reacktor bei Gasdurchgang. *Chem. Eng. Sci.* **1966**, *21*, 777−790.

(55) Linek, V.; Benes, P. Enhancement of oxygen absorption into sodium-sulfite solutions. *Biotechnol. Bioeng.* **1978**, *20* (5), 697−707.

(56) Augenstein, D. C. Oxygen absorption in fermentors at high power inputs. Ph.D. Thesis, Massachusetts Institute of Technology, Cambridge, MA, 1967.

(57) Laurent, A.; Charpentier, J.; Prost, C. Etude de la cinetique heterogene globale de l'oxidation catalytique d'une solution aqueuse de sulfite de sodium par l'oxygene gazeux en presence de sulfate de cobalt. *J. Chim. Phys.* **1974**, *71* (4), 613−614.

(58) Ogawa, S.; Shimizu, Y.; Tone, S.; Otake, T. Kinetics of the oxidation of aqueous sodium sulfite solutions with air. *J. Chem. Eng. Jpn.* **1982**, *15* (5), 400−402.

(59) Lamont, G.; Scott, D. An eddy cell model of mass transfer into surface of a turbulent liquid. *AIChE J.* **1970**, *16*, 513−519.

(60) Ditsch, A.; Laibinis, P. E.; Wang, D. I. C.; Hatton, T. A. Controlled clustering and enhanced stability of polymer-coated magnetic nanoparticles. *Langmuir* **2005**, *21* (13), 6006−6018.

(61) Moeser, G. D.; Roach, K. A.; Green, W. H.; Laibinis, P. E.; Hatton, T. A. Water-based magnetic fluids as extractants for synthetic organic compounds. *Ind. Eng. Chem. Res.* **2002**, *41* (19), 4739−4749.

(62) Calderbank, P. The interfacial area in gas−liquid contacting with mechanical agitation. *Trans. Chem. E* **1958**, *36*, 443−459.

(63) Van't Riet, K. Mass transfer in fermentation. *Trends Biotechnol.* **1983**, *1* (4), 113.